CHAPTER 9: Li_2O PARTICULATE FLOW CONCEPT – APPLE DESIGN

Contributors

Lead Author: Dai Kai Sze
Dai Kai Sze, Zhanhe Wang (ANL)
Mark. Tillack, David Zhang (UCSD)
Mohamed. Sawan, Hesham. Khater, I. Sviatoslavsky (UW)

9. LI_2O PARTICULATE FLOW CONCEPT – APPLE DESIGN

9.1 Introduction

The APEX (Advanced Power Extraction) and ALPS (Advanced Limiter-divertor Plasma-facing Systems) are two new programs in the US to investigate advanced, high performance blanket and divertor concepts. One of the goal is to be able to handle very high neutron wall loading and surface heat flux. One possible concept is to allow the coolant/breeding material to face directly the plasma.region.

The desirable material properties of the coolant/breeding material are,

1. Low vapor pressure at high temperature
2. Low activation
3. Good tritium breeding capability
4. Low electrical conductivity
5. High thermal conductivity
6. Low tritium solubility

The selection of the coolant/breeding material is a compromise among all these requirements. After reviewing the potential candidates of the available coolant/breeding materials, the solid breeder Li_2O was identified to have a good potential in fulfilling most of the above requirements.

Based on ITER assessment, the total vapor pressure over Li_2O is very low. At 1000ºC, the combined vapor pressure of all the possible components is about 10^{-5} torr. Therefore, the Li_2O can be heated up to a very high temperature without worrying about plasma containment. For comparison, the vapor pressure of lithium is 40 torr at the same temperature.

Both Li and O are low activation materials. The only activation product from lithium is tritium, which is required for the fuel of the D-T plasma. The activation from oxygen is very low.

Li_2O has good tritium breeding potential. This is partially due to the high lithium density in the Li_2O, which is higher than the lithium density in the pure lithium. This is only one of the few breeding material, which has the potential to sufficiently breed tritium without a neutron multiplier. With the low structural fraction in the APEX type design, the tritium breeding will not be a serious issue. Neutronics calculations, as described later in this report, confirm the tritium breeding capability.

Li_2O has very low electrical conductivity. Therefore, MHD will not have severe impact on the flow of the Li_2O stream. The thermal conductivity of Li_2O is rather low. This causes problem on removing surface heat, which will be the issue on the divertor and the first wall of the blanket. The heat transfer issue can be alleviated due to the high allowable surface

temperature of the Li_2O. Also, the increase in the Li2O particulate velocity will increase the heat removal capability of the Li_2O flow.

The tritium solubility in the Li_2O is rather low. The solubility reduces as the temperature of the Li_2O increases. Therefore, for high system like APEX, the tritium inventory in the blanket will be rather low.

9.2 Mechanical Design of Apple

9.2.1 General Configuration

The Apple concept relies on a granular flow of Li_2O particulates for breeding and cooling. The particulates flow from the top of the Tokamak chamber by gravity, falling all the way to the bottom and exiting there. At the first wall, the particulates are not constrained, but are in free fall with the bare granules in full view of the plasma. There are two configurations that have been considered, one with some baffles for flow control, and the other with no baffles. Each will be described separately.

9.2.1.1 Concept with Baffles

A concept using baffles for guiding the particulates was proposed from the start and as far as particulate flow and control, has an excellent chance of success. Figure 9.2.1-1 shows such a concept for a particular elongated plasma shape Tokamak. It shows an inlet for the particulates at the top where they are diverted to both sides of the chamber by a baffle. Some of the particulates follow the contour of the first wall while being directed by baffles at different locations. The remaining particulates flow in the back regions of the blanket where successive layers are retarded in flow commensurate with the nuclear heating at the particular depths. At the bottom, all the streams converge and exit through the bottom tube.

At the first wall, the particulates are in free fall, and one of the concerns is the rarefaction of the density of particulates due to acceleration. It has been thought that adding particulates at the first wall from slots along the height of the chamber can alleviate this condition, but requires experimental verification. In the divertor region, there are openings in the baffles to allow free access of ions to the particulates. The ions streaming along magnetic field lines would strike the falling particulates depositing their energy in turn, and in some cases, getting trapped in the Li_2O and being swept out of the chamber providing a means of pumping the unburned fuel.

Another thought that caught people's imagination is to allow the plasma to lean against the falling particulates at midplane as in a limiter, such that some of the ions in the scrape-off region can be intercepted before reaching the divertor. This would alleviate the heat load on the divertor and spread out the energy over a larger area of the particulates at the first wall.

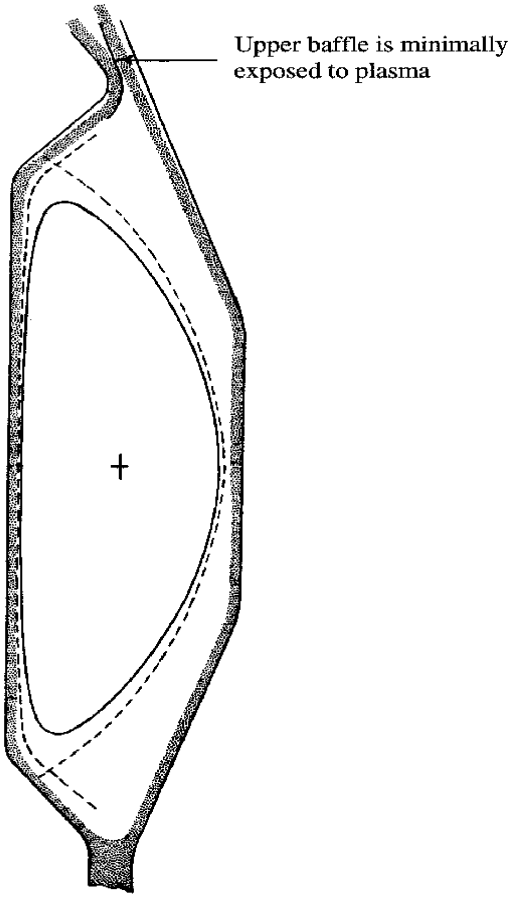

Figure 9.2.1-1. Li2O Flow Concept for an Elongated Plasma in a Tokamak

The most critical issue in the concept using baffles is the material used and its survivability. It is proposed that the structural material used in the Apple concept is SiC. However, because of its low thermal conductivity, it is doubtful that SiC can be used for the baffles. Another option is to use SiC for the blanket throughout, but use W plates for the baffles. The baffles are not subjected to high loads and therefore are not structural. Tungsten is a very high temperature material with high strength and can accommodate about a large MW/m^2 of surface heat load assuming that heat can be radiated from both sides of the baffle as well as conducted away on the back side by the particulates.

9.2.1.2 Concept without Baffles

It has been suggested that the baffles can be altogether eliminated by allowing the inertia of the particulates to carry them across the curved surfaces of the first wall. The most difficult part is at the top where the particulates are admitted into the chamber. Figure 9.2.1-2 shows such a possible configuration. There is one single baffle at the inlet, only partially exposed to the surface heat from the plasma. This curved baffle directs the flow to the inboard side of the chamber and then allows the particulates to flow with their own inertia

until they strike the inboard side wall, finally falling down the vertical distance to the bottom. Similarly on the outboard side, the particulates fall on an inclined slope and then continue by their own inertia until they meet the outboard sidewall. This concept assumes that the particulates can achieve the needed velocity in free fall at the top to have the inertia required to carry them across the open distance to the chamber walls. The biggest question is that the particulates cannot dribble down into the plasma from the lip of the baffle, which would be detrimental to the plasma. Therefore, this concept although interesting, will require considerable experimentation before it can be implemented.

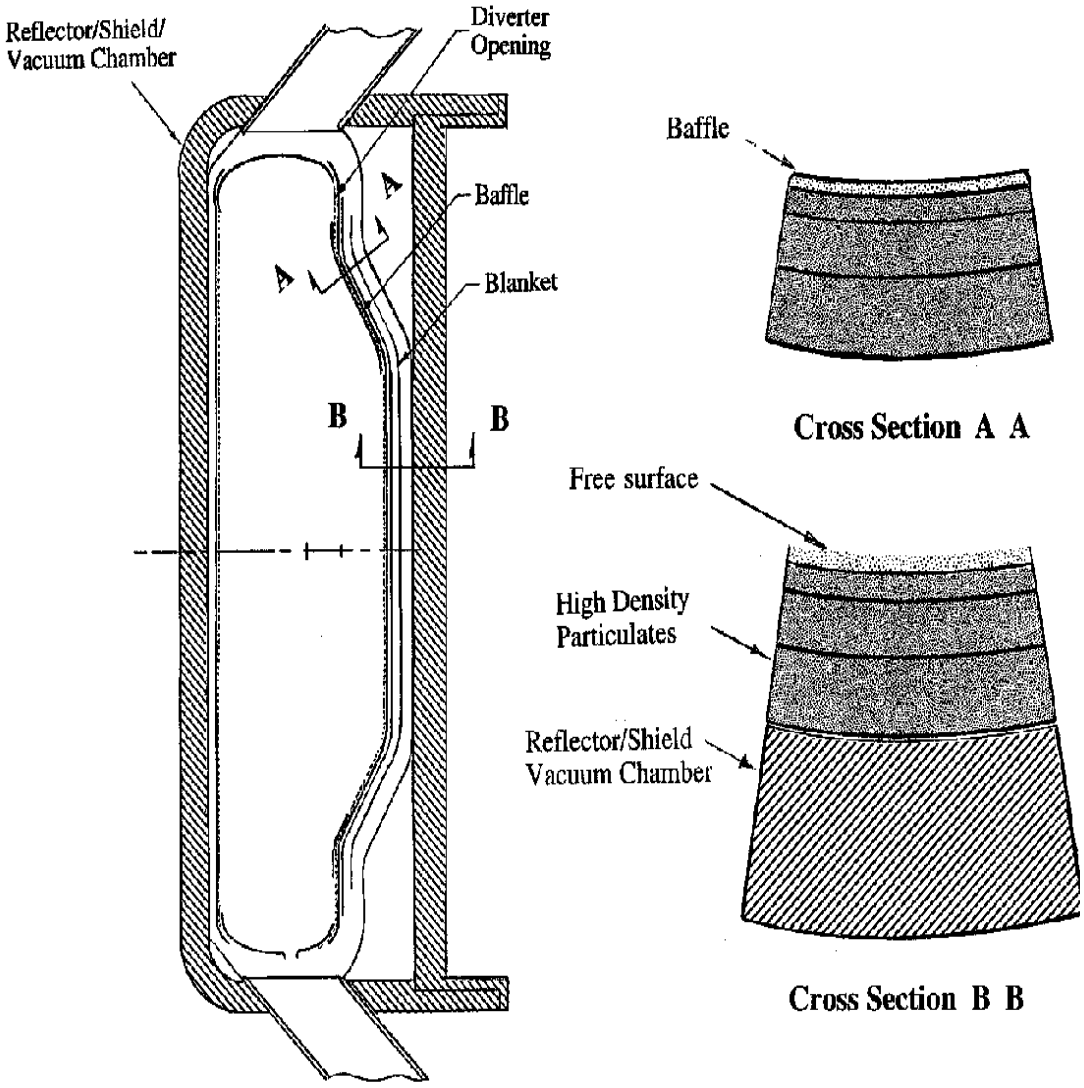

Figure 9.2.1-2. Li2O Particulate Flow Concept without Baffles

9.2.2 Accommodation of Penetration

There are primarily two shapes of penetration that may be needed for a Tokamak, rectangular as in the case of RF heating, and circular as for the neutral beams or pellet

injection. Figure 9.2.2-1 shows such penetrations provided through the particulate curtains at the first wall.

Providing such penetration again depends on baffles. Streamlining the penetration is needed to avoid abrupt changes in the direction of particulate fall. The particulate flow around the penetration must be smooth with no possibility of bouncing off in the wrong direction. Underneath the penetration, there must be deflectors to move the particulates back under the penetration in order to continue their downward flow. As in the other baffles, an issue here is their cooling. One possibility is to use deflectors in the vertical legs to slow down the particulates and fill the spaces between the baffle and the back wall with higher density particles and thus provide cooling in this way.

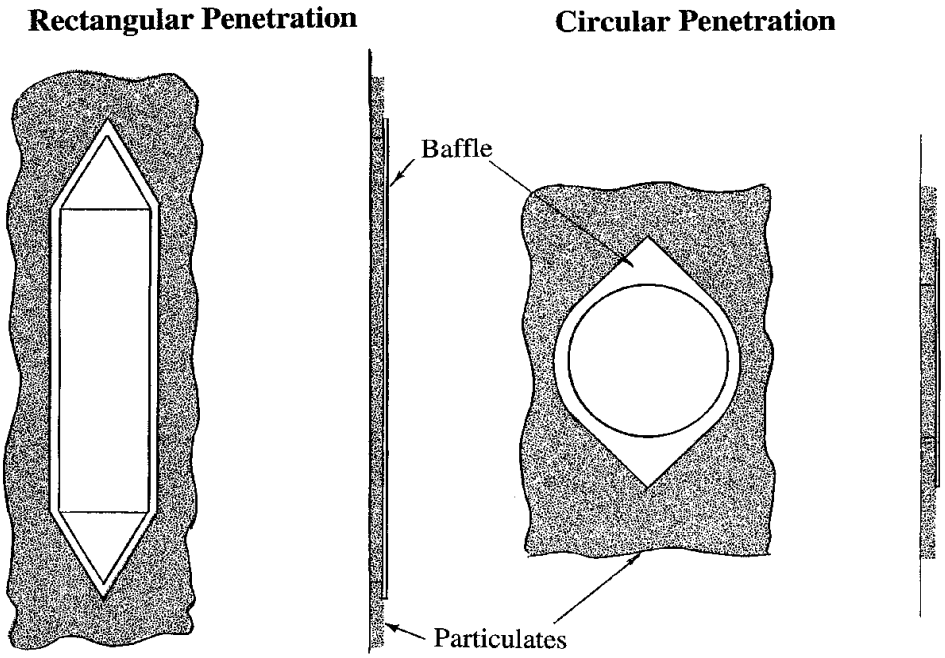

Figure 9.2.21 Several Shapes of Penetrations

9.2.3 Effect of Disruption

An interesting aspect of the Apple chamber design is its ability to handle plasma disruption. In the event of a disruption, the plasma current will transfer into the nearest conducting surface, which in this case is the metallic reflector/shield. This is a massive lifetime componenet that can withstand high JXB forces. The thermal components of the disruption will either impact the particulates or the baffles. If the particulates are impacted, some evaporation will take place or they may get accelerated and scattered around the chamber. In

the case of the baffles, SiC will also be ablated and some of the W surface may melt. Unless the baffles are damaged beyond use, recovery from a disruption should be relatively quick.

9.2.4 Maintenance of Exposed Apple Components

All the baffles are made of SiC or W. They are non-structural components that can withstand high radiation damage. These plasma-facing components will be designed for access and replacement through a special purpose port while vacuum integrity is maintained at the vacuum chamber wall. The upper breeder isolation values are closed, and the breeder material is drained through the bottom of the chamber. With the breeder removed, the empty blanket components are very light. The baffle studs are severed and replaced with new ones anchored to the reflector wall. The old baffles are removed and new baffles installed.

Replacing blanket modules can be performed in the usual way for Tokamaks either through parts in the upper region of the chamber or radially between TF coils.

9.3 Particle Dynamics

9.3.1 Introduction

Plasma-facing components, including the first wall and divertor, are subjected to very severe environmental conditions and must exhibit relatively high reliability and lifetime in a fusion power plant. Concerns include thermomechanical responses to high heat flux, plasma particle erosion, neutron damage and electromagnetic forces. The idea of using liquid plasma-facing surfaces was recognized from the early days of fusion power plant studies as a potential solution to many of these concerns [1]. A rather extensive R&D program in the former Soviet Union helped to develop several free surface liquid metal design concepts [2], and more recently the U.S. has embarked on an intensive program to explore a wider range of advanced in-vessel design concepts that includes free-surface liquids [3,4].

A potentially fatal flaw with liquid plasma-facing surfaces is the plethora of plasma interactions that are almost completely unknown. Evaporation of neutral atoms into the plasma edge will limit the operating temperature and power handling capability of liquids, and may lead to degraded and/or unpredictable plasma performance. MHD and transient electromagnetic interactions with the plasma are highly uncertain and complex. Previous attempts to introduce a liquid plasma-facing surface into tokamaks have found substantial impurity ingress and severe degradation of plasma performance [5,6].

Granular concepts have been considered for many years as an alternative coolant in confined channel flows [7] as well as a candidate for direct plasma exposure [8]. In addition to impurity control advantages, the surface heat flux handling capability of a fast-flowing stream of pebbles has been shown to exceed 100 MW/m^2 [9]. The main features of granular fluids that distinguish them from liquids include low vapor pressure, high temperature limits, absence of MHD and electromagnetic interactions, and also the ability to engineer the pebbles with multiple layers to satisfy plasma-interactive, tritium transport and heat removal requirements individually.

One of the most fundamental concerns with granular fluids is flow control - whether or not a granular medium can be injected and guided without a plasma-facing wall in such a way as to remove heat while maintaining acceptable performance without interfering with the plasma. Most of the difficulty with flow control stems from the lack of fluid cohesion. Some of the concerns include maintenance of adequate packing fraction, particle ejection into the plasma and flow around penetrations.

Figure 9.3.1-1 shows the cross section of a low aspect ratio (ST) power core with a granular first wall and divertor that served as the reference geometry for flow analysis. The flow is introduced from the top where it is guided by SiC baffles and allowed to free-fall into a collection zone at the bottom. Initial studies of granular flows have been performed on this geometry using particle dynamic simulations in several basic flow geometries: a straight vertical chute, a vertical chute fed by a hopper, and a vertical chute with curved back wall. These studies have shown a characteristic feature of these flows – compaction and its resulting internal contact forces invariably lead to decompaction and a tendency for the bed to separate. Fortunately, the requirement on bed packing fraction is very modest, such that even a few percent is adequate to intercept 99% of the plasma radiation heat flux.

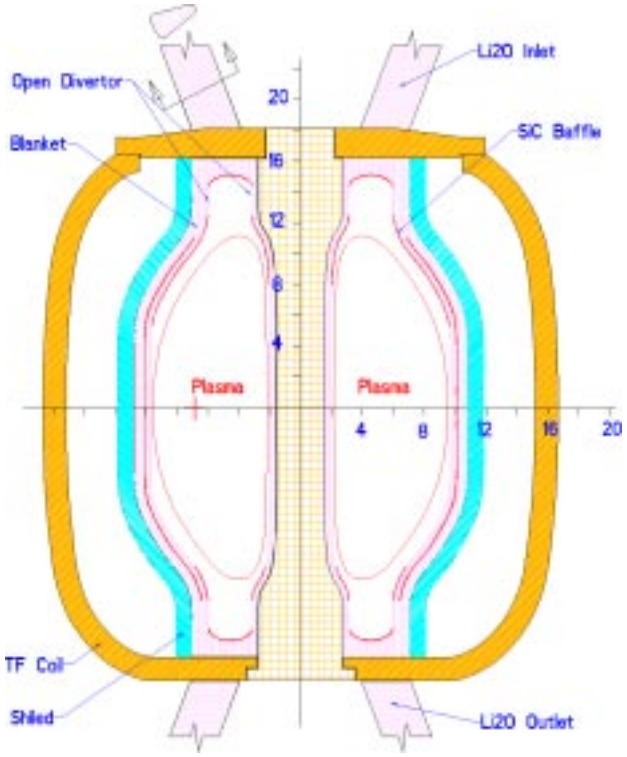

Figure 9.3.1-1 Cross-section of the APPLE concept

9.3.2 Analysis Method

9.3.2.1 Particle flow model

Particle dynamic simulation has seen a renaissance during the past several years due to computer advances that allow solutions of the equations of motion for large assemblages of particles. At present, commercially available codes are available for both 2D and 3D dynamic simulations. Using the PFC2D modeling tool [10], particle trajectories, contact forces and rotational motions have been studied for various inlet and downstream configurations.

PFC2D models the movement and interaction of stressed assemblies of circular particles using the distinct element method (DEM). The DEM was introduced originally by Cundall [11,12] for rock and soil mechanics problems, and has been applied extensively to the analysis of plug flows [13,14]. The interaction of particles is treated dynamically with states of equilibrium developing as the internal forces balance. The solution alternates between the application of Newton's second law to individual particles (to determine the motion of each particle arising from the contact and body forces acting upon it) and a force-displacement law at the contacts (to update the contact forces arising from the relative positions at each contact). The particles interact with each other and with walls only at contact points, using a soft-contact approach wherein the rigid particles are allowed to overlap one another. The small amount of overlap between the rigid bodies (see Figure 9.3.2-1) is related to the force by either a linear or Hertz-Mindlin relation. Both normal and shear forces are determined using the corresponding normal and shear stiffnesses:

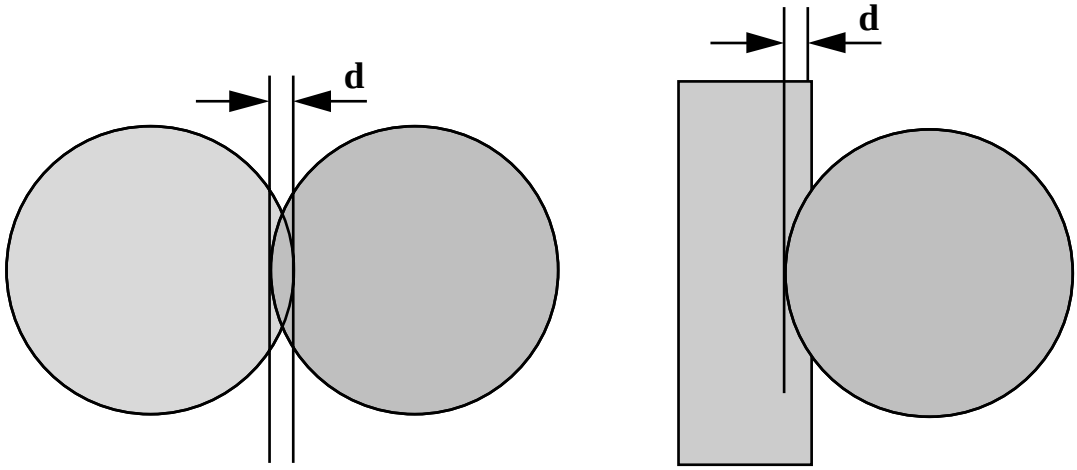

Figure 9.3.2-1. Contact between two spheres and between a sphere and a wall

$$F_i^n = K^n U^n n_I \quad (1)$$

$$\Delta F_i^s = -K^s \Delta U_i^n \quad (2)$$

where K^n and K^s are the normal and shear stiffness, respectively, and U^n and U^s are the normal and tangential overlap.

The translational and rotational motions of a single rigid particle are determined by the resultant force and moment vectors acting upon it. The equations for translational and rotational motion can be written in the vector form as:

$$F_i = m\,(d^2x_i/dt^2 - g_i) \quad (3)$$
$$M_i = dH_i/dt \quad (4)$$

where F_i is the resultant force, m is the mass, g_i is the acceleration of gravity, M_i is the moment, and H_i is the angular momentum of the particle.

9.3.2.2 Radiation opacity

One of the principal requirements on a free-surface granular flow is to intercept the majority of the plasma thermal radiation before it arrives at the first solid structural wall. A first-order estimate can be obtained using Bouger's Law applied to a uniform bed of depth 'd':

$$I = I_o \exp(-a_\lambda d) \quad (5)$$

where 'a_λ' is the spectral absorption coefficient. For spherical particles with radius 'r', number density 'n' and spectral absorption efficiency 'e_λ', the absorption coefficient can be expressed as [15]:

$$a_\lambda = \pi r^2 n e_\lambda \quad (6)$$

The bed porosity (ε) can be related to the number density of particles as follows:

$$\varepsilon = 1 - 4/3\,\pi r^3 n \quad (7)$$

Combining Eqns. 5–7 for a grey medium with e_λ=1, we find:

$$I/I_o = \exp(-3/4\,(1-\varepsilon)\,d/r) \quad (8)$$

For example, using pebbles with 0.5-mm radius, the product of packing fraction and bed depth must be at least 3 mm in order to reduce the time-averaged radiation heat flux by two orders of magnitude. This can be achieved with a 5-cm bed having 94% porosity or a 15-cm bed having 98% porosity.

9.3.3 Simulation Results And Discussion

9.3.3.1 Vertical Chute

In order to illustrate the basic flow characteristics of a free-falling bed, a simple vertical chute was examined first. For all cases examined, 2D cylinders with 1-mm diameter were simulated. The number of particles varied between 10,000 and 20,000, and a particle friction coefficient of 0.5 and various wall friction coefficients from 0.1–0.5 were used.

Conservation of mass dictates that the bed will decrease in effective thickness as its downstream velocity increases. Unlike liquids, the actual thickness tends to remain constant and the porosity increases proportionally with velocity. In free fall:

$$v^2(x) = v_o^2 + 2gx \tag{9}$$

The initial velocity should be larger than $(2gx)^{1/2}$ in order to avoid substantial reduction in downstream porosity. Friction with the walls can help decelerate the bed downstream, however excessive wall interactions can lead to particle scattering and/or over-compaction.

An initially uniform bed with uniform initial velocity has been shown to flow essentially as a slug (see Figure 9.3.3-1), which is a desirable outcome. The downstream porosity evolves consistent with Eq. 9. However, establishing the initial uniform condition is not easy in practice. Figure 9.3.2-2 shows the opposite extreme of a vertical chute, which is initially plugged near the channel exit. A compaction wave emanates from the obstruction and causes a buildup of internal contact forces. As particles on the downstream side of the compaction zone escape, they accelerate away from the bulk of the bed, leading to large increases in downstream porosity and erratic, nonuniform flow patterns. Clearly, the method of injection is one of the most important factors in determining the downstream conditions.

9.3.3.2 Flow From a Hopper

In order to examine more realistic inlet conditions, a simple hopper was modeled. Particles are fed into the top of the hopper and undergo some amount of densification as they accumulate. Particles then escape from an exit slot at the bottom. The exit slot width is chosen to be large enough to avoid complete bridging across the exit; however, internal contact forces always arise due to the angle of the walls with respect to gravity. As shown in Figure 9.3.3-3, a boundary layer appears on the walls near the throat and grows until it fills the throat region. The accumulation of contact forces in this region leads to substantial densification, followed by downstream porosity increase similar to the case of an initially plugged opening. The downstream porosity in this case is ~98%. As with the straight vertical chute cases, particle scattering is not seen to be a problem.

9.3.3.3 Flow Along a Curved Back Wall

Figure 9.3.3-4 shows an example of the effect of a curved back wall used to guide the flow. The fluid is given an initial velocity of 10 m/s at the inlet and subsequently piles up against the wall at the location where the curvature changes. A boundary layer clearly can be seen to grow from this location. Gravity acts on the flow so as to create an additional boundary layer on the tip of the front wall. Thus, one can observe interaction between the particles leaving the tip and the stagnated boundary flow on the back wall, resulting in substantial particle scattering. Such multiple compaction points are clearly something to be avoided.

Figure 9.3.3-1. Flow geometry in a vertical chute with uniform initial condition

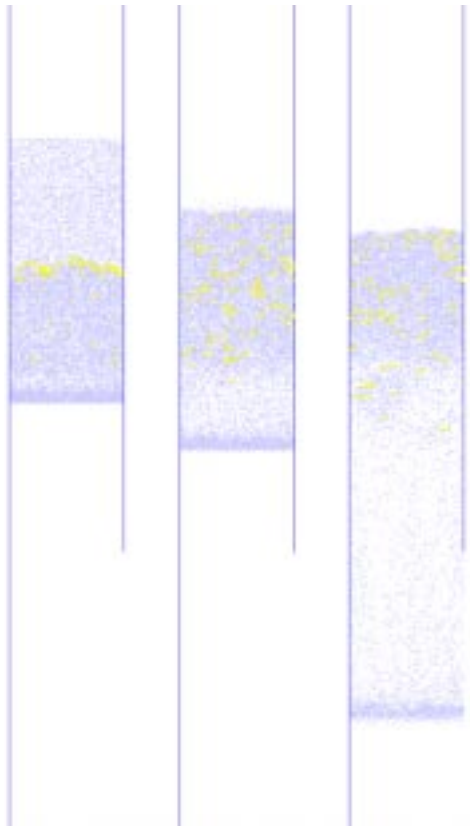

Figure 9.3.3-2. Flow geometry in a vertical chute with plugged initial condition

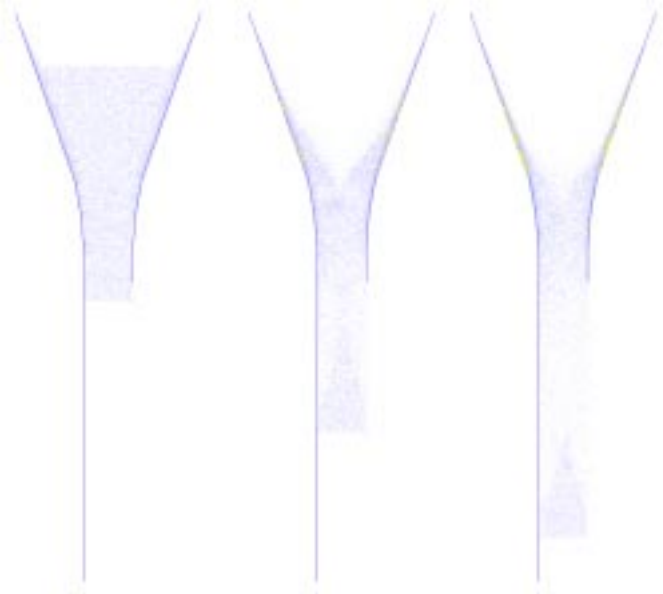

Figure 9.3.3-3. Flow from a hopper

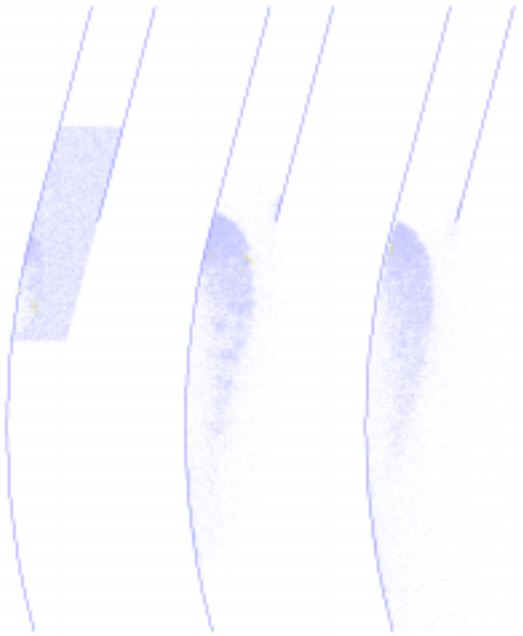

Figure 9.3.3-4 Flow along a curved wall

9.3.4 High Porosity Inlet Condition

The recognition that compaction and decompaction phenomena are likely to dominate the down stream flow behavior of free-surface granular flows suggests that the inlet porosity might be a dominant parameter. Higher initial porosity might lead to lower downstream porosity if internal contact forces can be avoided. In Figure 9.3.4-1, a hopper is underfilled with a higher porosity (0.96) as compared with the case shown in Figure 9.3.3-3 (0.92). The downstream boundary layer is evident, but does not grow to fill the entire flow path. A somewhat more uniform flow distribution results.

Figure 9.3.4-1. Flow from a high-porosity inlet condition

9.3.5 Conclusions

A variety of compaction, decompaction and scattering phenomena have been observed in the simulation of free-surface granular flows. In the absence of cohesive forces, contact forces are the dominant mechanism that determines the downstream porosity and trajectories. The existence of wall curvature or obstructions invariably leads to some amount of bed compaction, followed by decompaction. However, the modest requirement on bed porosity to adequately screen the first solid wall from plasma radiation appears to be achievable.

The presence of multiple compaction sites can lead to interactions that scatter particles away from the bed. Situations in which a realtively controlled flow is achievable have been observed; these generally require large radius of curvature and low friction coefficient. Careful control of the inlet conditions, including both the velocity and porosity, is a critical factor in achieving well-behaved downstream flows.

These initial studies have not definitively confirmed nor denied the existence of acceptable flow regimes in a real three-dimensional plasma chamber. Further numerical and experimental studies are needed, in combination with more detailed configurational designs.

9.4 Nuclear Analysis

9.4.1 Calculational Model

Neutronics and activation calculations have been performed for the APPLE concept. The local nuclear parameters were determined using a one-dimensional model in which both the inboard and outboard regions are modeled simultaneously to properly account for the toroidal geometrical effects. The plasma-facing layer is 5 cm thick with Li_2O at 30% packing. It is followed by a 0.5 cm thick SiC separation wall. The Li_2O in the blanket has a packing fraction of 0.6. The shield consists of 80% steel and 20% H_2O. The vacuum vessel is made of two steel sheets each 5 cm thick sandwitching a 30-cm-thick shielding zone made of 80% steel and 20% H_2O. While 316SS was used in the neutronics calculations, both 316SS and low activation ferritic steel were considered in the activation analysis. The results were normalized to outboard and inboard wall loadings of 10 and 7 MW/m^2, respectively. The local neutronics results were coupled with the appropriate coverage fractions to estimate the overall parameters. Neutron coverage fractions for the outboard, inboard, and divertor regions were assumed to be 75%, 15%, and 10%, respectively. The neutronics and shielding calculations were performed using the ONEDANT discrete ordinates code. The activation calculations were carried out using the activation code DKR-PULSAR2.0.

9.4.2 Blanket Optimization

The impact of blanket thickness on the local tritium breeding ratio (TBR) and energy multiplication (M) was investigated. The results in Fig. 9.4-1 show that the TBR increases with blanket thickness reaching a maximum value of 1.3. On the other hand, M decreases slightly (<8%)with increasing the blanket thickness reaching a minimum value of 1.1. The results are for natural lithium in the Li_2O. The effect of enriching Li in ^6Li is shown in Fig. 9.4-2. It is clear that

enriching the Li results in significant decrease in TBR and negligible increase in M. Therefore, natural Li is used in the reference APPLE design.

In addition to breeding tritium and multiplying the fusion energy, the Li_2O particulate blanket in the APPLE concept is required to reduce the damage rate in the structural material of the shield to allow it to be a lifetime component. The peak damage rate in the shield depends on the blanket thickness. Fig. 9.4-3 gives the impact of blanket thickness on the peak damage and gas production rates in the shield structure. The steel damage and gas production rates decrease by an order of magnitude for each 35 cm of blanket thickness. Assuming 30 full power years (FPY) plant lifetime and a 200 dpa damage limit for the steel structure, a minimum blanket (Li_2O @ 60% packing fraction) thickness of 40 cm is required for the structure to be lifetime component. Based on these results, the inboard blanket thickness in the reference design is taken to be 40 cm. On the other hand, with the less constrained space on the outboard side, a 75-cm-thick outboard balanket is utilized in the reference design to enhance the overall tritium breeding potential. Notice that further increase in blanket thickness results only in modest TBR increase as shown in Fig. 9.4-1.

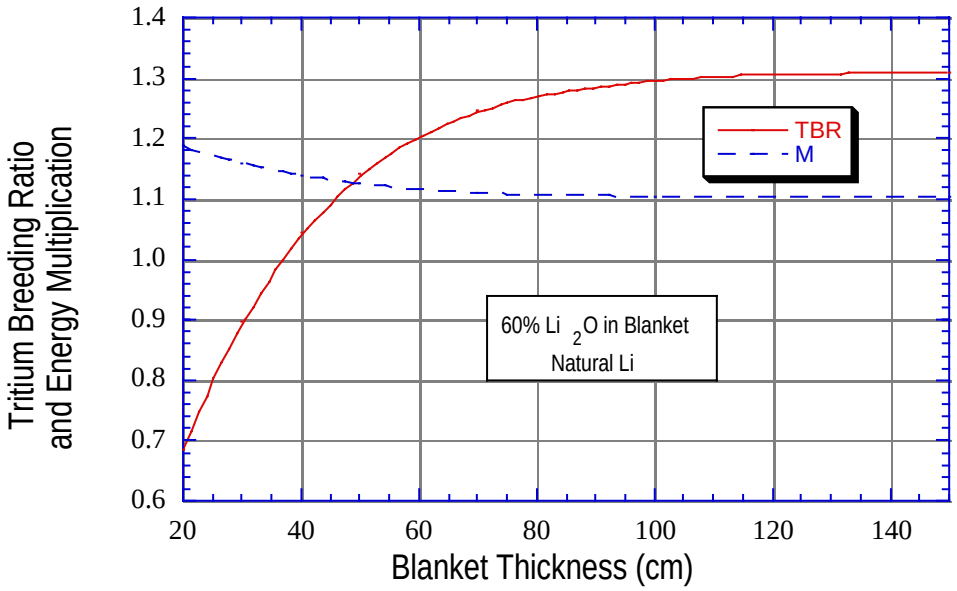

Fig. 9.4-1. Impact of blanket thickness on local tritium breeding ratio and energy multiplication.

9.4.3 Tritium Breeding and Energy Multiplication

The local TBR and M values obtained in the reference design are given in Table 9.4-1. The results are shown for both the inboard and outboard regions. Only 3.2% of nuclear heating in the outboard region is deposited in the water-cooled shield and vacuum vessel. In the inboard side, the shield and vacuum vessel contribute 15.4% of the nuclear heating.

The overall TBR and M depend on the neutron coverage fractions (NCF) of the regions surrounding the plasma and the blanket thickness in each region. The relative NCF for the inboard and outboard regions varies significantly with the aspect ratio. Fig. 9.4-4 shows the variation of the outboard NCF with the reactor aspect ratio. To estimate the overall TBR and M, we assumed neutron coverage fractions of 75%, 15%, and 10% for the outboard, inboard, and divertor regions, respectively, corresponding to an aspect ratio of 2.5.

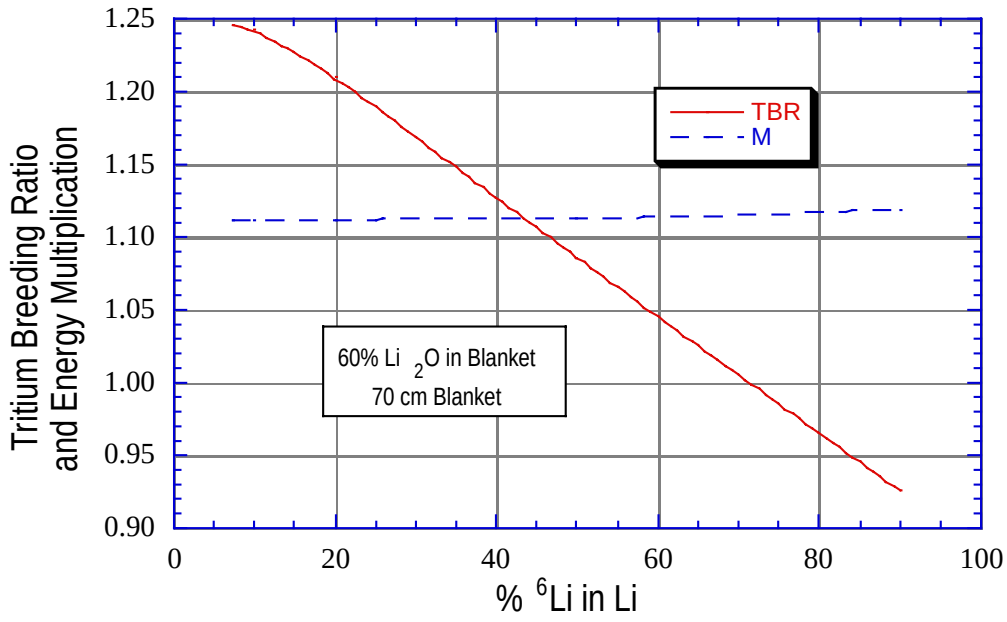

Fig. 9.4-2. Effect of lithium enrichment on local tritium breeding ratio and energy multiplication.

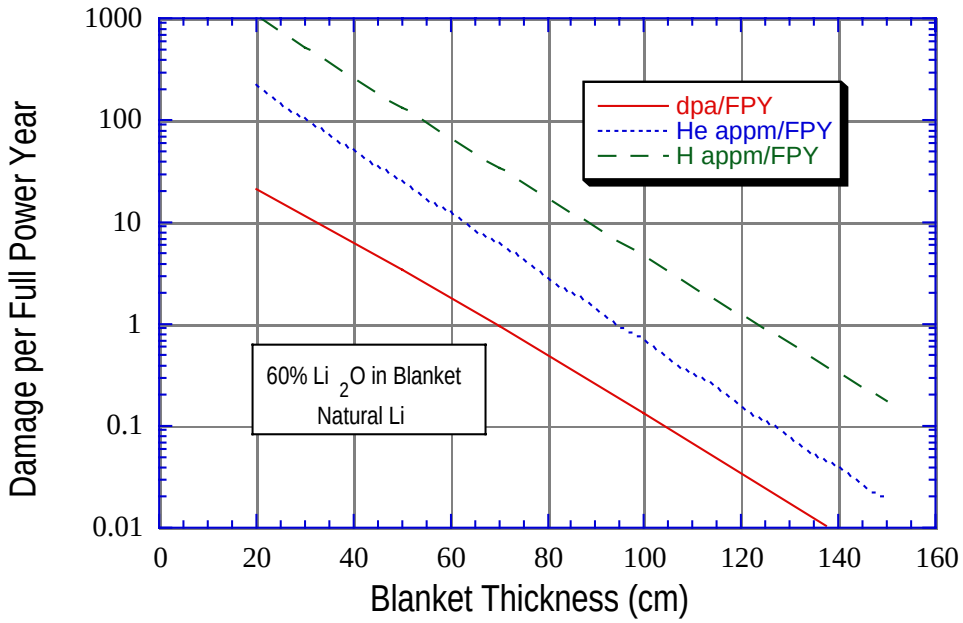

Fig. 9.4-3. Impact of blanket thickness on peak damage and gas production rates in the steel structure of the shield.

Table 9.4-1. Local TBR and M in the reference APPLE design.

	Inboard	Outboard
Total Blanket Thickness (cm)	40	75
Local TBR	1.158	1.233
Local M	1.166	1.099

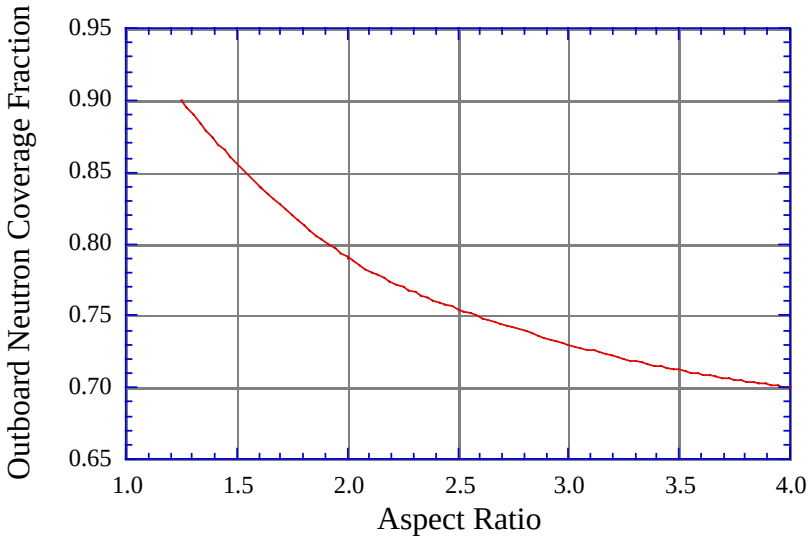

Fig.9.4-4. Impact of aspect ratio on outboard neutron coverage fraction

The local TBR and M values were combined with neutron coverage fractions to determine the overall TBR and M. The blanket thickness in the divertor region is assumed to be 40 cm as that in the inboard region. The overall TBR is estimated to be 1.215. The outboard, inboard, and divertor regions contribute 76.2%, 14.3%, and 9.5%, respectively. The overall energy multiplication is estimated to be 1.116. 93.6% of the nuclear heating is deposited as high grade heat in the Li_2O particulate blanket.

9.4.4 Nuclear Heating and Radiation Damage

The peak power density and damage rate values in the SiC separation wall are given in Table 9.4-2. The results are given for the inboard and outboard regions. Both the atomic displacement and helium production rates are given. The damage rates are high and frequent replacement will be needed. Notice that the SiC baffles and separation walls do not contain pressure and are not structure members. The lifetime for these non-structural components is not defined. The baffles and separation walls in the APPLE concept are designed for quick replacement.

Table 9.4-2. Nuclear heating and damage rate in the SiC separation wall.

	Inboard	Outboard
Peak Nuclear Heating (W/cm^3)	54.9	75.0
Peak dpa Rate (dpa/FPY)	72.8	93.1
Peak He Prod. Rate (He appm/FPY)	7310	10438

The steel structure of the shield located behind the Li_2O particulate blanket experiences lower nuclear heating and damage rate due to neutron attenuation in the blanket. Table 9.4-3 gives the peak power density and radiation damage values in the steel structure at the back of the blanket. The results are given for both the inboard and outboard regions. Nuclear heating and radiation damage values in the outboard region are much lower than in the inboard region due to the larger attenuation in the thicker outboard blanket. The peak cumulative atomic displacement damage after 30 FPY plant life is less than the 200 dpa limit considered for steel structure. This implies that the steel structure at the back of the Li_2O particulate blanket in the APPLE concept is expected to be a lifetime component.

Table 9.4-3. Peak nuclear heating and radiation damage in the steel structure.

	Inboard	Outboard
Peak Nuclear Heating (W/cm^3)	14.9	4.3
Peak dpa rate (dpa/FPY)	5.54	0.87
Peak end-of-life dpa @ 30 FPY	166.2	25.9
Peak He Prod. Rate (He appm/FPY)	42.6	5.5
Peak end-of-life He appm @ 30 FPY	1277	163

9.4.5 Vacuum Vessel and Magnet Shielding

The vacuum vessel (VV) is located behind the shield. The vacuum vessel consists of two steel sheets each 5 cm thick sandwitching a 30-cm-thick shielding zone made of 80% steel and 20% H_2O. For the vacuum vessel to be reweldable, the cumulative helium production in the structure should not exceed 1 He appm. The shield thickness needed to reduce the peak helium production in the vacuum vessel to less than 1 He appm after 30 FPY plant life was determined. Adequate VV shielding is provided using a 40-cm-thick outboard shield and a 55-cm-thick inboard shield. The shield is assumed to consist of 80% steel and 20% H_2O. Table 9.4-4 gives the peak neutronics parameters for the VV in both the inboard and outboard regions. The results clearly indicate that the VV is reweldable.

Table 9.4-4. Peak VV neutronics parameters

	Inboard	Outboard
Peak Nuclear Heating (mW/cm^3)	10	11
Peak end-of-life dpa	0.09	0.10
Peak end-of-life He appm	0.40	0.42

Adequate shielding must be provided for the superconducting magnets such that their performance is not degraded by neutron and gamma radiation. The component most sensitive to radiation is the organic insulator because of possible degradation in mechanical strength. Radiation damage could also affect the critical properties of the superconductor and the resistivity of the copper stabilizer. In addition magnet nuclear heating that is removed by cryogenic liquid helium should be limited. We will assume that the magnet radiation limits are similar to those adopted in the ITER design. These are end-of-life fast neutron fluence of 10^{19} n/cm^2, end-of-life dose to the insulator of 10^9 Rads, $6x10^{-3}$ end-of-life dpa to Cu stabilizer, and 1 mW/cm^3 peak nuclear heating. Table 9.4-5 gives the peak radiation effects in the magnet located behind the 40-cm-thick VV. It is clear that all magnet radiation limits are satisfied.

9.4.6 Radial Build for the Reference Design

The outboard radial build that satisfies requirements for steel structure lifetime, vacuum vessel reweldability, and superconductor magnet shielding is 155 cm (75 cm blanket, 40 cm shield, and 40 cm VV). In the inboard region, the total radial build is 135 cm (40 cm blanket, 55 cm shield, and 40 cm VV). This radial build is shown in Fig. 9.4-5. This configuration also allows for tritium self-sufficiency with the overall TBR estimated to be 1.215.

Table 9.4-5. Peak magnet neutronics parameters

Parameter	**Inboard**	**Outboard**	**Design Limit**
Peak Nuclear Heating (mW/cm^3)	0.028	0.027	1
Peak end-of-life Fast Neutron Fluence, E> 0.1 MeV (n/cm^2)	$8.5x10^{17}$	$8.0x10^{17}$	10^{19}
Peak end-of-life Dose to Epoxy Insulator (Rads)	$8.3x10^8$	$7.1x10^8$	10^9
Peak end-of-life dpa to Cu Stabilizer	$4.3x10^{-4}$	$4x10^{-4}$	$6x10^{-3}$

	Li_2O @ 30% p.f.	SiC wall	Li_2O @ 60% p.f.	Shield 80% Steel 20% H_2O	Steel	VV 80% Steel 20% H_2O	Steel
Thick (cm)							
IB	5	.5	34.5	55	5	30	5
OB	5	.5	69.5	40	5	30	5

Fig. 9.4-5. Radial build for the reference APPLE design

9.4.7 Decay Heat and Activation

9.4.7.1 Introduction

Activation analysis was performed for the APPLE concept. Calculations are performed assuming neutron wall loadings of 7 and 10 MW/m^2 at the inboard and outboard first walls, respectively. The analysis used the ORNL low activation ferritic steel (LAFS) 9Cr-2WVTa as a structure material. The elemental composition of the ferritic steel 9Cr-2WVTa alloy is shown in Table 9.4-6. A 0.5 cm thick separation wall separates the Li_2O in the plasma facing layer from the blanket. The separation wall is made of a SiC composite. Based on dpa limits for SiC, the separation wall (baffle) was assumed to be replaced every 2 FPY. On the other hand, the shield and vacuum vessel were assumed to stay in place for 30 FPY. Neutron transport calculations were performed using the discrete ordinates neutron transport code DANTSYS. The neutron flux obtained from the neutron transport calculations was used in the activation calculations. The activation analysis was performed using the activation code DKR-PULSAR2.0. The code combined the neutron flux with the FENDL/A-2.0 data library to calculate the activity and decay heat as a function of time following shutdown. Calculated specific activities were used to calculate the waste disposal ratings (WDR) of the different components at the end of their life-time. Results of the decay heat analysis were used to evaluate the temperature variation exhibited by the structure during a loss of coolant accident (LOCA).

9.4.7.2 Activity and decay heat

Figures 9.4-6 and 9.4-7 show the specific activity and decay heat values induced in the different components of APPLE as a function of time following shutdown, respectively. As shown in the two figures, the ORNL LAFS produces acceptable level of radioactivity after shutdown. The inboard and outboard shields dominate the overall activity and decay heat induced

in the structure. Table 9.4-7 shows a list of nuclides that dominate the induced radioactivity in the different components. As shown in the table, $^{55}Fe(T_{1/2} = 2.7$ yr), $^{185}W(T_{1/2} = 75.1$ day), and $^{187}W(T_{1/2} = 23.9$ hr) are the main contributors to the induced radioactivity during the first few weeks following shutdown. $^{55}Fe(T_{1/2} = 2.7$ yr) and ^{54}Mn dominate the induced activity in the intermediate-term following shutdown. The long-term radioactivity (between one and 10 years) is mostly generated by the $^{63}Ni(T_{1/2} = 100$ yr) and $^{60}Co(T_{1/2} = 5.27$ yr) isotopes. Nuclides with much longer half-lives have no impact on the decay heat generated from the LOCA point of view. However, as shown in the next section, these nuclides dominate the waste disposal ratings.

Table 9.4-6. Elemental Composition of the ORNL LAFS Alloy.

Nuclide	wt% or wppm
C	0.1%
Si	0.25%
V	0.025%
Cr	9%
Mn	0.5%
Fe	88.055%
Co	34 wppm
Ni	402 wppm
Nb	0.5 wppm
Mo	70 wppm
Pd	0.18 wppm
Ag	0.16 wppm
Cd	0.05 wppm
Eu	0.05 wppm
Dy	0.05 wppm
Ho	0.05 wppm
Er	0.05 wppm
Ta	0.07%
W	2%
Os	0.02 wppm
Ir	0.05 wppm
Bi	0.05 wppm

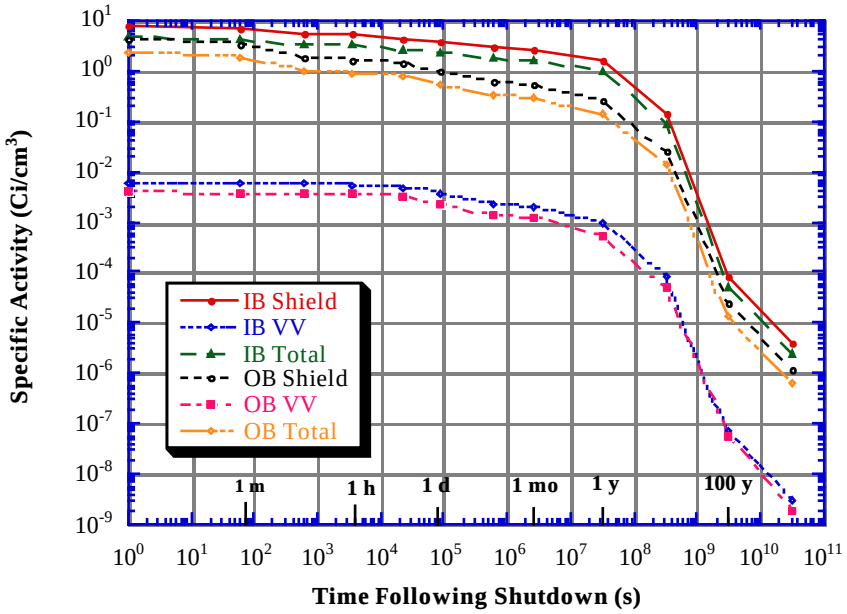

Fig. 9.4-6. Activity induced in the different components of APPLE as a function of time following shutdown

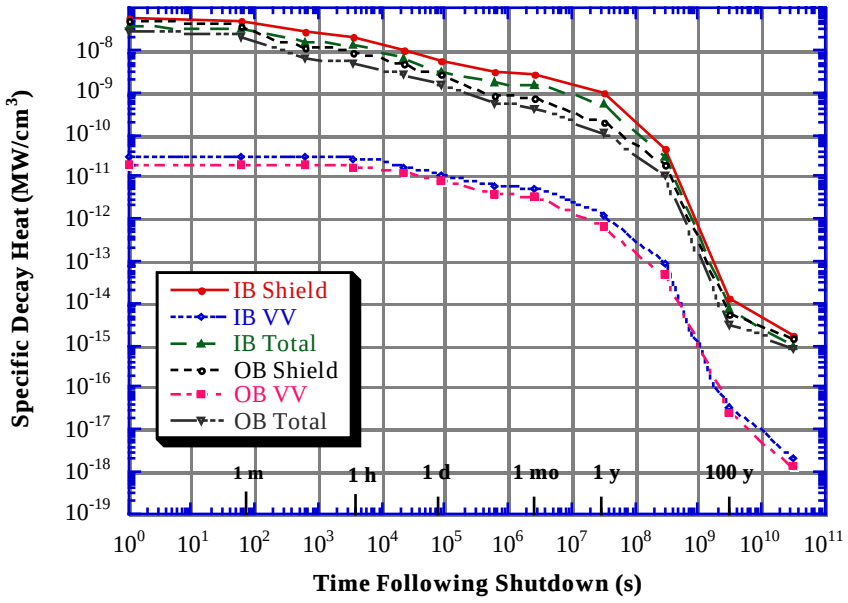

Fig. 9.4-7. Decay heat induced in the different components of APPLE as a function of time following shutdown

Table 9.4-7. List of Dominant Nuclides.

	Activity	Decay Heat
Short-term < 1 day	^{55}Fe, ^{185}W, ^{187}W	^{56}Mn, ^{187}W
Intermediate-term < 1 month	^{55}Fe, ^{54}Mn, ^{51}Cr	^{54}Mn, ^{182}Ta
Long-term > 1 year	^{55}Fe, ^{63}Ni	^{60}Co, ^{54}Mn

9.4.7.3 Waste disposal ratings

The radwaste of the different components of APPLE were evaluated according to both the NRC 10CFR61 and Fetter waste disposal concentration limits (WDL). The 10CFR61 regulations assume that the waste disposal site will be under administrative control for 100 years. The dose at the site to an inadvertent intruder after the 100 years is limited to less than 500 mrem/year. The waste disposal rating (WDR) is defined as the sum of the ratio of the concentration of a particular isotope to the maximum allowed concentration of that isotope taken over all isotopes and for a particular class. If the calculated WDR = 1 when Class A limits are used, the radwaste should qualify for Class A segregated waste. The major hazard of this class of waste is to individuals who are responsible for handling it. Such waste is not considered to be a hazard following the loss of institutional control of the disposal site. If the WDR is > 1 when Class A WDL are used but = 1 when Class C limits are used, the waste is termed Class C intruder waste. It must be packaged and buried such that it will not pose a hazard to an inadvertent intruder after the 100 years institutional period is over. Class C waste is assumed to be stable for 500 years. Using Class C limits, a WDR > 1 implies that the radwaste does not qualify for shallow land burial.

Fetter developed a modified version of the NRC's intruder model to calculate waste disposal limits for a wider range of long-lived radionuclides which are of interest for fusion researchers than the few that currently exist in the current 10CFR61 regulations. Fetter's model included more accurate transfer coefficients and dose conversion factors. However, while the NRC model limits the whole body dose to 500 mrem or the dose to any single organ (one of seven body organs) to 1.5 rem, Fetter limits are based on the maximum dose to the whole body only.

Specific activities calculated by the DKR-PULSAR2.0 code were used to calculate the waste disposal ratings (WDR). The waste disposal ratings for the Fetter and 10CFR61 limits are shown in Tables 9.4-8 and 9.4-9, respectively. Results in the tables are given for compacted wastes. Compacted waste corresponds to crushing the solid waste before disposal (to eliminate voids in the structure) and thus disallowing artificial dilution of activity. The Class C WDR were calculated after a one-year cooling period. The dominant nuclides are given between brackets. As shown in Table 9.4-8, according to Fetter limits, all components would qualify for disposal as

Class C waste. The source for the WDR of the SiC baffle is the $^{26}Al(T_{1/2} = 7.3 \times 10^5$ yr) isotope which is produced by ^{28}Si (n,t) reaction. On the other hand, $^{192m}Ir(T_{1/2} = 240$ yr), and $^{94}Nb(T_{1/2} =$ 20,000 yr) are the dominant source of WDR for all other components. They are produced by nuclear interactions with the iridium, niobium and molybdenum impurities present in the ORNL LAFS alloy. Finally, as shown in Table 9.4-9, according to the 10CFR61 limits, all components also would qualify for disposal as Class C waste. Except for the WDR of SiC baffle, which is dominated by the $^{14}C(T_{1/2} = 5730$ yr) isotope, the waste disposal ratings of all other components are dominated by contribution from the ^{94}Nb isotope.

Table 9.4-8. Class C Waste Disposal Ratings Using Fetter Limits.

Zone	FPY	WDR	Dominant Nuclides
SiC Baffle	2	0.275	^{26}Al
Inboard Shield	30	0.648	^{192m}Ir, ^{94}Nb
Inboard VV	30	4.54×10^{-3}	^{192m}Ir
Outboard Shield	30	0.46	^{192m}Ir, ^{94}Nb
Outboard VV	30	4.39×10^{-3}	^{192m}Ir

Table 9.4-9. Class C Waste Disposal Ratings Using 10CFR61 Limits.

Zone	FPY	WDR	Dominant Nuclides
SiC Baffle	2	0.02	^{14}C
Inboard Shield	30	0.144	^{94}Nb
Inboard VV	30	1.92×10^{-4}	^{94}Nb
Outboard Shield	30	0.057	^{94}Nb
Outboard VV	30	1.86×10^{-4}	^{94}Nb

References

[1] B. Badger, *et al.*, "UWMAK-I, A Wisconsin Toroidal Fusion Reactor Design," University of Wisconsin Report UWFDM-68 (1974).

[2] E. Muraviev, *et al.*, "Liquid Metal Cooled Divertor for ARIES," General Atomics report, GA-A21755, UC-420, Jan. 1995.

[3] R. F. Mattas, *et al.*, "US Assessment of Advanced Limiter-divertor Plasma-facing Systems (ALPS) - Design, Analysis, and R&D Needs," *Fusion Technology* 34 (3), Part 2 (Nov. 1998) 345–350.

[4] M. A. Abdou and the APEX Team, "Exploring novel high power density concepts for attractive fusion systems," *Fusion Engineering & Design* 45 (1999) 145-167.

[5] V. O. Vodyanyuk, *et al.*, "Liquid Metal Tokamak Limiter. Problem Definition and First Results," *Plasma Physics* 14 (5) 1988, p. 628.

[6] S. V. Mirnov, V. N. Dem'yanenko, and E. V. Murav'ev, "Liquid-metal tokamak divertors," *Journal of Nuclear Materials* 196-198 (1992) 45-49.

[7] R. E. Nietert and S. I. Abdelk-Khalik, "Thermal hydraulics of flowing particle-bed-type fusion reactor blankets," *Nuclear Eng. & Design* 68 (3), 1981, p.293-300.

[8] K. H. Burrell, "A Method of Removing Helium Ash and Impurities from Fusion Reactors," *J. Fusion Energy* 1 (3) 1981.

[9] M. Isobe, K. Matsuhiro, Y. Ohtsuka, Y. Ueda, and M. Nishikawa, "Conceptual Design of Pebble Drop Divertor," 17th IAEA Fusion Energy Conference (Yokohama 1998), to be published in *Nuclear Fusion*.

[10] "Distinct Element Particle Flow Codes PFC2D and PFC3D," Itasca Consulting Group, Inc., Minneapolis MN, 1998.

[11] P. A. Cundall, "Formulation of a Three-Dimensional Distinct Element Model-Part I. A Scheme to Detect and Represent Contacts in a System Composed of Many Polyhedral Blocks", *Int. J. Rock Mech., Min, Sci. & Geomech. Abstr.*, 25 (3), p.107-116.

[12] R. Hart, P. A. Cundall, and J. Lemos, "Formulation of a Three-Dimensional Distinct Element Model-Part II. Mechanical Calculations for Motion and Interaction of a System Composed of Many Polyhedral Blocks", *Int. J. Rock Mech., Min, Sci. & Geomech. Abstr.*, 25 (3), p.117-125.

[13] Y. Tsuji and R. Asano, "Fundamental Investigation of Plug Conveying of Cohesionless Particles in a Vertical Pipe (Pressure Drop and Friction of Stationary Plug)", Can. J. Chem. Eng., Vol. 68, (1990), p.758-767.

[14] T. Kawaguchi, T. Tanak, and Y. Tsuji, "Quasi-Three-Dimensional Numerical Simulation of Vertical Plug Flows", Proc. of the 5th World Congress of Chemical Engineering, Vol. 6, San Diego, USA, July, (1996), p.481-486.

[15] R. Siegel and J. R. Howell, "Thermal Radiation Heat Transfer", Third Edition, Hemisphere Publishing Corporation, p.660.